AB

Katholieke *Universiteit* Nijmegen

Nijmegen preprint
HEN-363
July 1994

TRANSVERSE MOMENTUM COMPENSATION IN $\pi^+ p$ INTERACTIONS AT 250 GeV/c

EHS/NA22 Collaboration

Nijmegen preprint
HEN-363
July 1994

TRANSVERSE MOMENTUM COMPENSATION IN π^+p INTERACTIONS AT 250 GeV/c

EHS/NA22 Collaboration

N.M. Agababyan[9], I.V. Ajinenko[5], H. Białkowska[8], P.V. Chliapnikov[5], F. Botterweck[4,a], M. Charlet[4,b], E.A. De Wolf[1,c], K. Dziunikowska[2,d], A.M.F. Endler[6], Z.C. Garutchava[7], H.R. Gulkanyan[9], D. Kisielewska[2,d], W. Kittel[4], K. Olkiewicz[2,d], F.K. Rizatdinova[3], E.K. Shabalina[3], L.N. Smirnova[3], J. Stepaniak[8], L.A. Tikhonova[3], A.G. Tomaradze[7], A. Wróblewski[8], F. Verbeure[1], S.A. Zotkin[4]

[1] Department of Physics, Universitaire Instelling Antwerpen, B-2610 Wilrijk and Inter-University Institute for High Energies, B-1050 Brussels, Belgium
[2] Institute of Physics and Nuclear Techniques of Academy of Mining and Metallurgy and Institute of Nuclear Physics, PL-30055 Krakow, Poland
[3] Nuclear Physics Institute, Moscow State University, RU-119899 Moscow, Russia
[4] University of Nijmegen/NIKHEF, NL-6525 ED Nijmegen, The Netherlands
[5] Institute for High Energy Physics, RU-142284 Protvino, Russia
[6] Centro Brasileiro de Pesquisas Fisicas, 22290 Rio de Janeiro, Brazil
[7] Institute of High Energy Physics of Tbilisi State University, GE-380086 Tbilisi, Georgia
[8] University of Warsaw and Institute for Nuclear Studies, PL-00681 Warsaw, Poland
[9] Institute of Physics, AM-375036 Yerevan, Armenia

Abstract. Compensation of transverse momentum is studied in π^+p interactions at 250 GeV/c. Significant $\vec{p}_T$-transfer is found between c.m.s. hemispheres. With respect to the beam axis transverse momentum is compensated over the whole event, with respect to the sphericity axis mainly within one hemisphere. The highest $\vec{p}_T$ in the event is mainly compensated by increased multiplicity. The QGSM and FRITIOF models qualitatively reproduce these effects, but important differences are observed.

---

[a] Now at Univ. Instelling Antwerpen
[b] EC guest scientist
[c] Onderzoeksleider NFWO, Belgium
[d] Supported by the Polish State Committee for Scientific Research

1 Introduction

Besides the longitudinal direction of a high energy collision, the transverse plane contains important information on the production mechanism. Of particular interest for the construction of parton models is the way in which transverse momentum $\vec{p}_T$ is compensated within the final state of a collision. In early studies [1], $\vec{p}_T$ was found to be compensated over a range in rapidity compatible with the total rapidity range available.

In [2] it has been shown that mini-jets with $|\vec{p}_T|$ more than a few GeV/c become important at energies exceeding ISR energies. Many authors have suggested that, at high energies, mini-jets are responsible not only for the global properties, such as the rapid increase of the total cross-section and the average charge multiplicity, but also for local correlations, such as fluctuations of multiparticle production and the mechanism of $\vec{p}_T$-compensation [3-12]. To trace possible differences in the particle production mechanism, it is interesting to compare $\vec{p}_T$-compensation in inclusive reactions with that in events with high p_T-production.

An elegant method to study $\vec{p}_T$ compensation in detail has been suggested in [13] and applied to heavy ion collisions in [14]. In this paper, the method proposed in [13] is used for π^+p-interactions at 250 GeV/c. The role of individual particles is studied in the compensation of the total $\vec{p}_T$ in each hemisphere, with respect to the beam, as well as to the sphericity axis. In addition, compensation of the highest $\vec{p}_T$ in the event is investigated. A related analysis in terms of longitudinal and transverse collective variables is performed in [15].

Two versions of the FRITIOF model (FRITIOF6.0 and FRITIOF7.0) and the Quark-Gluon-String Model (QGSM) are used for comparison with the experimental data.

In Sect.2, the experimental procedure and the statistics used for the analysis are presented. Section 3 contains a brief description of the models. The method is recalled and the data are compared with the model predictions in Sect. 4. Conclusions are given in Sect. 5.

2 The experiment

The experiment has been performed with the European Hybrid Spectrometer (EHS), using a meson-enriched beam from the SPS accelerator. The analysis is based on results of the reconstruction of events in the hydrogen filled rapid cycling bubble chamber RCBC, used as a vertex detector, and a downstream spectrometer. A detailed description of the experimental set-up is given in [16, 17] and references therein.

Events are accepted when measured and reconstructed charge multiplicity are consistent, charge balance is satisfied and no electron is detected. Only events with all tracks satisfying our quality criteria are included in this analysis. Two-prongs are excluded.

For momenta $p_{LAB} < 0.7$ GeV/c, the range in the bubble chamber and/or the change of track curvature is used for proton identification. In addition, a visual ionization scan has been used for $p_{LAB} \leq 1.2$ GeV/c on 62 % of the π^+p sample. Particles identified as protons are given proton mass. Particles with momenta $p_{LAB} > 1.2$ GeV/c are not identified in the present analysis and are treated as pions.

Single diffractive events (from π^+ or p dissociation) are defined as events of charged particle multiplicity $n \leq 6$ with at least one positive particle having Feynman $|x_F| \geq 0.88$ and are removed from the sample.

After these cuts, our sample consists of 41.533 non-single-diffractive π^+p events with charged particle multiplicity $n > 2$. A correction is applied for the loss of events during measurement and reconstruction by normalization to the topological cross section data [16]. The average charge multiplicity of inelastic non-single diffractive events is 9.23±0.14 [18].

3 Quark models

A comparison is performed with three models: the Lund type models FRITIOF6.0 [19] and FRITIOF7.0 [20] and the Quark-Gluon-String model QGSM [21].

The FRITIOF mechanism of producing particles can be characterized as "total diffraction", in which each of the colliding particles is excited to form a dipole. During the collision between the two hadrons, many uncorrelated momentum transfers occur. This leads to a reaction of the evolving strings as if they had been worked upon by a single momentum transfer. The color separation causes gluonic bremsstrahlung. The beam meson fragments like a quark-antiquark chain in e^+e^--annihilation and the target-nucleon dipole like a quark-diquark chain in lepton-nucleon collisions. In both versions, default parameters are used (e.g. mean primordial p_T^2 for string ends equal to 0.25 $(\mathrm{GeV/c})^2$ for version 6.0 and 0.30 $(\mathrm{GeV/c})^2$ for version 7.0, width of the Gaussian transverse momentum distribution for primary hadrons $\sigma_x = \sigma_y = 0.35$ GeV/c and 0.405 GeV/c, respectively).

The main difference between versions 6.0 and 7.0 is that hard (Rutherford) parton scattering is included in 7.0, but not in 6.0.

The QGSM is based on dual topological unitarization. In addition to 2 strings being formed between valence quark and antiquark and between quark and diquark of the colliding hadrons, respectively, strings are formed between sea quarks and antiquarks of the primordial particles. The string breaking algorithm of QGSM is described in [21]. At the string break-up, the transverse momenta of the sea quark $\vec{p}_T$ and antiquark $-\vec{p}_T$ are assumed to be distributed according to $P(p_T^2) = 3b/[\pi(1 + b\vec{p}_T^2)^4]$ with $b = 0.34(GeV/c)^{-2}$. The diquark from the proton compensates the total transverse momentum of the other quarks (antiquarks). Due to an increase of the number of quark-gluon strings with increasing energy, the average p_T of quarks and antiquarks, and via the compensation that of the diquark, increases. The transverse momentum of valence quarks is distributed according to $P(p_T^2) = c\exp(-cp_T^2)/\pi$ with a slope parameter $c = 10$ $(\mathrm{GeV/c})^{-2}$. QGSM does not include any hard parton scattering.

The main differences between the models used for comparison with the experimental data are colour exchange (present in QGSM, but not in FRITIOF) and hard parton scattering included only in FRITIOF7.0. So, a comparison of the experimental data with model predictions is expected to elucidate the role of hard processes and the role of colour exchange at our energies. All three models give reasonable descriptions of the gross features of the data in terms of multiplicity, single particle p_T and rapidity distributions,

and as such can be used as background for observation of any multi-jet effects or any other phenomena in p_T-generation. Rather than attempting to tune the models to the data presented in this paper, we restrict ourselves to a comparison in terms of the default parameters. Retuning of the parameters on the basis of *all* NA22 results is foreseen in later stage.

Two-prong and diffractive events are excluded from the Monte Carlo events by the same cuts as used for the data. Proton misidentification is treated as in the data.

4 Results

4.1 Transverse momentum compensation between hemispheres

The total transverse momentum of charged particles in one cms hemisphere gives a first estimate of typical p_T-values of groups of particles. It sets the scale of any collective effects in the transverse plane. Neglecting neutral particles, total transverse momentum vectors $\vec{Q}_b$ and $\vec{Q}_f$ are defined over all charged particles in backward (proton) and forward (π^+) hemispheres, respectively, as

$$\vec{Q}_b = \sum_{j=1}^{k} \vec{p}_{T,j} \quad , \quad \vec{Q}_f = \sum_{j=k+1}^{n} \vec{p}_{T,j} \quad , \tag{1}$$

where n is the total number of charged particles in the event and k that of charged particles in the backward hemisphere. The average values of the magnitudes of $\vec{Q}_f$ and $\vec{Q}_b$ are presented in columns 2 and 3 of Table 1, together with the corresponding model predictions. The values of $\langle Q_f \rangle$ and $\langle Q_b \rangle$ (≈ 1 GeV/c) observed are significantly larger than the average transverse momentum of single particles and also larger than expected from FRITIOF and QGSM. The former means that significant $\vec{p}_T$-exchange takes place between hemispheres, the latter that there is significantly more $\vec{p}_T$-exchange between hemispheres in the data than in the models.

A difference exists between the $\langle Q_f \rangle$ and $\langle Q_b \rangle$ values in columns 2 and 3 of Table 1. This difference is explained from neutral particles not included in the analysis, since otherwise $\vec{Q}_b = -\vec{Q}_f$ would follow for every event from momentum conservation.

Fig. 1 shows the distribution in the azimuthal angle $\Delta\varphi$ between $\vec{Q}_f$ and $\vec{Q}_b$. A deviation from $\Delta\varphi = \pi$ means that the role of neutral particles is not negligible. However, even when including neutrals, transverse momentum conservation imposes some constraints on the $\Delta\varphi$ distribution. A simple statistical model can be constructed, in which $\frac{d\sigma}{d\Delta\varphi}$ can be derived analytically. The three vectors $\vec{Q}_f$, $\vec{Q}_b$ and the total transverse momentum of neutrals $\vec{Q}_o$ must sum up:

$$\vec{Q}_f + \vec{Q}_b + \vec{Q}_o = 0 \quad . \tag{2}$$

Let us assume the same Gaussian ansatz for each $\vec{Q}$ vector. Then the differential cross section can be written in the form:

$$\frac{d\sigma}{d\vec{Q}_f d\vec{Q}_b d\vec{Q}_o} = \prod_i \exp(-bQ_i^2)\delta^{(2)}(\sum \vec{Q}_i) \quad . \tag{3}$$

We assume the same value of b for $\vec{Q}_f$, $\vec{Q}_b$ and $\vec{Q}_0$, which seems reasonable, as the average multiplicity of neutral pions is approximately 1/2 of charged ones. Using a Fourier representation of the $\delta^{(2)}$ function and performing the integration over all variables except the azimuthal angle $\Delta\varphi$ between any two $\vec{Q}$ vectors, one gets (independent of the value the parameter b) [22]:

$$\frac{d\sigma}{d\Delta\varphi} = \frac{3}{4\pi(1-x^2)}[\frac{x}{(1-x^2)^{1/2}}(\arcsin(x) - \frac{\pi}{2}) + 1] \quad , \tag{4}$$

where $x = \frac{1}{2}\cos\Delta\varphi$. Thus, in the statistical model the angular correlation between $\vec{Q}_f$ and $\vec{Q}_b$ does not depend on the magnitude of the $\vec{Q}$ vectors. The $\frac{d\sigma}{d\Delta\varphi}$ distribution calculated according to this formula is shown in Fig.1 as dotted line. It provides a satisfactory description of the data (taking into account the deficiency of the approximation used).

Model predictions are presented as dot-dashed line (FRITIOF6.0), full line (FRITIOF 7.0) and dashed line (QGSM) and are also in agreement.

To understand how the transverse momentum is distributed inside the two hemispheres and to understand the role of the central region, we distinguish particles from the central region ($\mid x_F \mid < 0.2$) and define the vectors $\vec{Q}_f$ and $\vec{Q}_b$ for this region, separately. The average values of the vectors $\vec{Q}_f$ and $\vec{Q}_b$ in this region are presented in columns 4 and 5 of Table 1. Differences between $\langle Q_f \rangle$ and $\langle Q_b \rangle$ can now be due to neutral particles and to the asymmetry of the x_F distribution of charged particles. The models also underestimate the total transverse momentum in the central regions.

Large $\vec{p}_T$-exchange between the two hemispheres leads to strong correlations between the values of $\langle Q_f \rangle$ and $\langle Q_b \rangle$. In Fig. 2, the dependence $\langle Q_f(Q_b) \rangle$ and $\langle Q_b(Q_f) \rangle$ is presented for all charged particles, as well for particles in the central region, together with the model predictions. The models are below the experimental points for all values of Q_f and Q_b. This is in agreement with the observation made for the averages in Table 1, but does not of itself mean that the correlations must also come out too low in these models. Indeed, an increase of $\langle Q_f \rangle$ and $\langle Q_b \rangle$ with increasing Q_b and Q_f, respectively, is seen for data *and* models.

To give a qualitative estimate of the strength of the correlation effect, we fit the observed increase by the usual linear functions

$$\langle Q_f \rangle = a_b + b_b\, Q_b \quad , \quad \langle Q_b \rangle = a_f + b_f\, Q_f \quad , \tag{5}$$

excluding the first points. Results of the fits are presented in Table 2. Strong positive correlations (measured by the slope b) are observed in the experiment between the total hemispheres, as well as in the central region. For the total hemisperes, FRITIOF6.0 underestimates the slopes, while in QGSM and FRITIOF7.0 the slopes are in agreement with experiment. All models underestimate the slope in the central region.

The correlation between the values of Q_f and Q_b is influenced by the correlation between the number of particles produced into the forward and backward hemispheres. Assuming absence of $\vec{p}_T$-correlations inside a hemisphere and neglecting transverse momentum conservation, one can derive the relation

$$\langle Q_b^2 \rangle = \langle (\sum_{j=1}^{k} \vec{p}_{T,j})^2 \rangle = k \langle p_T^2 \rangle \quad . \tag{6}$$

For the case that the $\langle p_T^2 \rangle$ of particles in the forward hemisphere is independent of that in the backward hemisphere, one can expect the same strength of correlation between Q_b^2 and Q_f^2 as for $\langle n_b(n_f) \rangle$. These forward-backward multiplicity correlations have been studied in our experiment in [23]. The slopes of $\langle Q_b^2(Q_f^2) \rangle$ and $\langle Q_f^2(Q_b^2) \rangle$, for the total hemispheres, as well as for the central region, are presented in Table 3, together with the model predictions and with the slopes for the forward-backward multiplicity correlations. A strong positive correlation is observed between Q_b^2 and Q_f^2 defined for the total hemispheres. A comparison of the correlation strength in Q^2 and n shows that the parameter b is much larger when evaluated in Q^2. The strength of correlation in n increases when limiting the analysis to the central region, but the difference remains very big even there. The models underestimate the slopes.

Since the forward-backward multiplicity correlations are weaker than the $Q_b^2(Q_f^2)$-correlations, one can conclude that a correlation exists between p_T-values of particles from different hemispheres. A comparison of experimental slopes with model predictions shows a big discrepancy between models and experiment for the central region and for the total hemispheres.

So, significant transfer of $\vec{p}_T$ is observed between forward and backward hemispheres in the cms, larger than predicted by FRITIOF and QGSM. The $\vec{p}_T$-transfer is mainly absorbed by the large number of particles produced in the central region. This means that the mechanism of multiparticle production leads to a collective effect of large-p_T groups of particles in the central region. No such mechanism exists in the models examined. Semi-hard processes, such as mini-jet production, could be responsible for this effect.

4.2 $\vec{p}_T$-compensation in inclusive reactions

In this section, we study the role of individual charged particles in $\vec{p}_T$-compensation, within the same and between opposite hemispheres. The projections of $\vec{p}_T$ on to the $\vec{Q}_b$ and $\vec{Q}_f$ - directions are calculated for each particle. In order to remove a distortion resulting from the projection of the particle momentum on to itself, vectors $\vec{Q}_{f,i}$ and $\vec{Q}_{b,i}$ are defined for each particle i by the sum over the remaining particles in a given hemisphere as

$$\vec{Q}_{b,i} = \sum_{j \neq i=1}^{k} \vec{p}_{T,j}, \qquad \vec{Q}_{f,i} = \sum_{j \neq i=k+1}^{n} \vec{p}_{T,j} \ . \tag{7}$$

We study the components of the transverse momentum in the direction of $\vec{Q}_{f,i}$ and $\vec{Q}_{b,i}$,

$$p_{1,i} = \vec{p}_{T,i} \cdot \frac{\vec{Q}_{f,i}}{|\vec{Q}_{f,i}|}, \qquad p_{2,i} = \vec{p}_{T,i} \cdot \frac{\vec{Q}_{b,i}}{|\vec{Q}_{b,i}|}, \tag{8}$$

(with $p_{1,i}$ or $p_{2,i}$ set to zero when $|\vec{Q}_{f,i}|$ or $|\vec{Q}_{b,i}|$ is zero, respectively). The component of $\vec{p}_{T,i}$ in the direction of the residual transverse momentum of a hemisphere gives information to what extent $\vec{p}_{T,i}$ of particle i is compensated in that hemisphere.

In Fig. 3 the dependence of $\langle p_{1,i} \rangle$ and $\langle p_{2,i} \rangle$ on the particle's rapidity y is shown for all charged particles, in comparison with the models. Small, but negative values of $\langle p_{1,i} \rangle$ and $\langle p_{2,i} \rangle$ are observed in the full rapidity region, indicating some compensation of $\vec{p}_{T,i}$

over the whole event. Small values of $\langle p_{1,i} \rangle$ and $\langle p_{2,i} \rangle$ mean that, on average, the direction of $\vec{p}_{T,i}$ of particle i correlates only weakly with the direction of the residual transverse momentum of a hemisphere. The largest negative values are observed in that hemisphere in which particle i is produced. So, compensation of a particle's transverse momentum is stronger in its own hemisphere than in the opposite hemisphere, but the difference is not large. The models follow the trend of the experimental data, but significant differences are observed, in particular for FRITIOF7.0.

In addition, a vector $\vec{Q}_i$ is defined as the difference,

$$\vec{Q}_i = \vec{Q}_{f,i} - \vec{Q}_{b,i} \quad . \tag{9}$$

Apart from the transverse momentum of neutral particles, $\vec{Q}_i$ corresponds to the transverse momentum transmitted from one hemisphere to the other.

In Fig. 4, the transverse momentum component in the direction of $\vec{Q}_i$,

$$p_{x,i} = \vec{p}_{T,i} \cdot \frac{\vec{Q}_i}{|\vec{Q}_i|} \quad , \tag{10}$$

is averaged over all charged particles of given y in all events and the dependence of $\langle p_{x,i} \rangle$ on the particle rapidity y is studied in the cms. The shape of the distribution for $|y| \lesssim 2.5$ is a consequence of definition (9) and (10) and reflects the fact seen in Fig. 3 that the $\vec{p}_T$-compensation of the given particle ($|y| \lesssim 2.5$) in his own hemisphere is stronger than in the opposite hemisphere.

The particles in the bin centred at $y = -2.8$, mainly the final state proton, are negatively correlated with the direction of $\vec{Q}_i$. This shows the important role of the relatively large transverse momentum of the proton in the $\vec{p}_T$ compensation. Except for this, the models approximately reproduce the trend of the data.

In tracing effects originating from local (essentially within one hemisphere) and from global (between the two hemispheres) $\vec{p}_T$-compensation, it is interesting to compare the results obtained with respect to the beam axis to those obtained with respect to the sphericity axis. By definition, effects of global p_T exchange between initial particles are suppressed in an analysis with respect to the latter.

The sphericity frame $\langle p_{1,i}^{sph} \rangle$ and $\langle p_{2,i}^{sph} \rangle$ distributions, are compared with the models in Fig. 5, where now y is defined with respect to the sphericity axis. The forward hemisphere w.r.t. the sphericity axis is chosen at random event by event, so that the $p_{1,i}^{sph}$ and $p_{2,i}^{sph}$ distributions are forced to follow:

$$\langle p_{1,i}^{sph}(y) \rangle = \langle p_{2,i}^{sph}(-y) \rangle \quad .$$

The component of $\vec{p}_{T,i}$ in the direction of the residual transverse momentum of the *same* hemisphere is negative and has larger absolute value than in Fig. 3. All models roughly describe the $\vec{p}_T$-compensation inside the hemisphere of the detected particle i, but the model curves are broader in y than the data. On the other hand, the component of $\vec{p}_{T,i}$ in the direction of the *opposite* hemisphere is small in the models, but has clearly positive values in experiment.

The average of component $p_{x,i}^{sph}$ in the sphericity system is shown in Fig. 6 as a function of rapidity y along the sphericity axis. The random choice of the forward direction here defines the form of the distribution to follow $\langle p_{x,i}^{sph}(y)\rangle = -\langle p_{x,i}^{sph}(-y)\rangle$. Indeed, in the new basis, the picture of compensation changes, for experiment as well as for the models. The values of $\langle p_{x,i}^{sph}\rangle$ at $|y| \approx 2-3$ are much larger than those of $\langle p_{x,i}\rangle$ in Fig. 4 and $\vec{p}_T$ exchange is considerably larger in experiment than in the models. The differences between the models themselves are largely reduced.

Transfer of $\vec{p}_T$ between forward and backward hemispheres becomes more evident in the new (sphericity) basis. A particle which compensates the residual transverse momentum of the own hemisphere is positively correlated with the direction of the total transverse momentum of the opposite hemisphere. Absence of these positive correlations in the models shows that $\vec{p}_T$-exchange between hemispheres is smaller in the models than in experiment.

So, the role of a particle in the compensation of the total transverse momentum of its own hemisphere becomes more essential when evaluated in the new basis than with respect to the beam axis (Figs. 5, 6 as compared to Figs. 3, 4). Long-range positive correlations become evident between a single particle from one hemisphere and the total $\vec{p}_T$ of the opposite hemisphere (Fig. 5). Both FRITIOF versions and QGSM qualitatively describe the experimental data, but the models predict a $\vec{p}_T$-compensation region wider in y than observed in experiment (Fig. 5). In the models practically no long-range positive correlations are expected between $\vec{p}_{T,i}$ of a particle from one hemisphere and the direction of the total $\vec{p}_T$ of the opposite hemisphere (Fig. 5).

4.3 High-p_T compensation analysis

To study the properties of production of particles with transverse momentum larger than average, the compensation of the highest charged particle transverse momentum in the event is investigated with respect to the sphericity axis. Only events with at least one charged particle (trigger) with $p_T > 1.5$ GeV/c are accepted in the analysis. To exclude distortion of the p_T-distribution by fast particles from the fragmentation regions and by phase space limitations, only triggers with $\mid y \mid < 2.0$ are accepted. The cross section of selected events (1065 events) is given in column 2 of table 4.

For the selected events, the vectors $\vec{Q}_{f,tr}$ and $\vec{Q}_{b,tr}$ are defined for triggers w.r.t. the sphericity axis. In Fig. 7, $\langle p_{1,tr}^{sph}\rangle$ and $\langle p_{2,tr}^{sph}\rangle$ are shown as a function of the trigger rapidity, and $\langle p_{x,tr}^{sph}\rangle$ in Fig. 8. Due to the random choice of the forward hemisphere similar symmetry properties are expected for Figs. 7 and 8 as observed in Figs. 5 and 6. Due to limited statistics, these properties are not perfect here. In Fig. 7, a deep minimum is observed in the trigger hemisphere. This means that all other particles within the trigger hemisphere tend to compensate the large $\vec{p}_T$ of the trigger. Only small positive correlations are observed between the $\vec{p}_T$ of the trigger and the total $\vec{p}_T$ of particles in the opposite hemisphere. QGSM reproduces the trend in the experimental data, but not FRITIOF.

A detailed analysis of trigger compensation is useful in tracing semi-hard processes in multiparticle production and is performed in the following w.r.t. the beam axis.

A comparison of global event characteristics with model predictions of FRITIOF and QGSM are presented in Table 4. The average charge multiplicity $\langle n \rangle$ is larger in events containing a particle with $p_T > 1.5$ GeV/c than the $\langle n \rangle \approx 9.23 \pm 0.14$ observed for our inelastic non-single diffractive events in [18]. Reasonable agreement is observed between experiment and QGSM. FRITIOF6.0 cannot reproduce the cross section. On the other hand, FRITIOF7.0, which includes hard parton scattering, underestimates their multiplicity.

Let us now define a transverse momentum flow as the sum of transverse momentum components in the trigger direction over all charged particles in an event, at given rapidity distance Δy to the trigger,

$$L(\Delta y) = \sum_{\substack{\text{charged} \\ \text{particles} \\ \text{at } \Delta y}} p_T \cos \Delta\varphi \ .$$

Here, $\Delta\varphi$ is the azimuthal angle between the trigger and the particle. The transverse momentum flow averaged over all events is shown in Fig. 9 as a function of Δy, separately for negative and positive particles, along the trigger direction in the transverse plane ($\Delta\varphi < \pi/2$) and in opposite direction ($\Delta\varphi > \pi/2$). The distributions have a maximum at small Δy. FRITIOF6.0 predicts far too small a flow of positive particles in both directions. Near the trigger ($\Delta y \lesssim 2$) also QGSM and FRITIOF7.0 underestimate the p_T flow of positives in both directions. Also for negatives none of the models is able to describe the flow simultaneously for $\Delta\varphi < \pi/2$ and $\Delta\varphi > \pi/2$.

The discrepancies in L may be connected with deviations between models and experiment in the average transverse momentum flow per particle, $\langle p_T \cos \Delta\varphi \rangle$, or in number of particles following the trigger or going into the opposite direction. The analysis of $\langle p_T \cos \Delta\varphi \rangle$ in Fig. 10 shows practically no dependence on Δy. The average values are $\langle p_T \cos \Delta\varphi \rangle \approx 0.2$ in the whole region of Δy for particles in the trigger direction and $\langle p_T \cos \Delta\varphi \rangle \approx 0.3$ for particles in the opposite direction. The models overestimate these values for negative particles.

In Fig. 11 the number of positive and negative particles (not including the trigger) is presented in the trigger direction and in the opposite direction. All models underestimate the number of positive particles in both directions. QGSM describes the number of negatives reasonably well, but both FRITIOF versions are too flat.

From figs. 9,10,11 it follows, that the trigger p_t is compensated mainly by a large number of particles with average p_T, emitted opposite to the trigger direction. This result agrees with observations made in [24] in terms of transverse energy (see also the model argumentation of [25]). The details of the compensation mechanism are not accounted for by the models considered in our analysis.

The charge flow $\langle n^+ - n^- \rangle$ along the trigger (not including the trigger) and in opposite direction is shown in Fig. 12, together with the model predictions. Both FRITIOF6.0 and QGSM, not including hard parton scattering, underestimate the charge flow opposite to the trigger. FRITIOF7.0 describes the experimental data very well. It has, however, been verified that this success is not due to the presence of hard scattering in the latter.

5 Conclusions

An analysis has been performed of transverse momentum compensation in π^+p-interactions at 250 GeV/c. The main results can be summarized as follows.

1. Significant transverse momentum transfer is observed between cms hemispheres. The transfer is larger than predicted by FRITIOF or QGSM. The transfer is mainly absorbed by the large number of particles in the central region.

2. Non-trivial correlations (beyond the multiplicity effect) exist between the total $\vec{p}_T$ of charged particles in forward and backward hemispheres.

3. Transverse momentum compensation with respect to the sphericity axis mainly takes place within one hemisphere. The models predict a compensation region wider in y than observed in experiment.

4. The analysis of the compensation of the highest $\vec{p}_T$ (>1.5 GeV/c) shows that the large $\vec{p}_T$ of the trigger is compensated mainly by particles in the trigger hemisphere.

5. The analysis of events with a trigger particle shows that the average charge multiplicity of such events is larger than that for all events. Significant flow of $\vec{p}_T$ and number of particles is observed along the trigger direction in the transverse plane and in opposite direction. This means that the high-$\vec{p}_T$ compensation is local in y-range and the mechanism of high-$\vec{p}_T$ production leads to collective effects. Neither of the examined models can reproduce these effects in detail, but QGSM is in better agreement with experiment than FRITIOF.

6. Within FRITIOF, a large cross section for high p_T trigger events can be obtained only by FRITIOF7.0, where hard parton scattering is included. So, hard processes cannot be neglected even at our energies.

Acknowledgments

We are grateful to the III. Physikalisches Institut B, RWTH Aachen, Germany, the DESY-Institut für Hochenergiephysik, Zeuthen, Germany, the Department of High Energy Physics, Helsinki University, Finland for early contributions to this experiment. This work is part of the research programme of the "Stichting voor Fundamenteel Onderzoek der Materie (FOM)", which is financially supported by the "Nederlandse Organisatie voor Wetenschappelijk Onderzoek (NWO)". We thank further NWO for support of this project within the programme for subsistence to the former Soviet Union (07-13-038).

References

1. D. Drijard et al.: Nucl. Phys. B155 (1979) 269
2. G. Albajar et al., UA1 Coll.: Nucl. Phys. B309 (1988) 405
3. A. Capella, J. Tran Thanh Van: Z. Phys. C23 (1984) 165
4. P. l'Heureux et al.: Phys. Rev. D32 (1985) 1681
5. G. Pancheri,Y.N. Srivastava: Phys. Lett. B182 (1986) 199
6. L. Durand, H. Pi: Phys. Lett. 58 (1987) 303; Phys. Rev. D38 (1988) 78
7. J. Dias de Deus, J. Kwiecinski: Phys. Lett. B196 (1987) 537
8. T.K. Gaisser, F. Halzen: Phys. Rev. Lett. 54 (1985) 1754
9. R.C. Hwa: Phys. Rev. D37 (1988) 1830
10. X.N. Wang, R.C. Hwa: Phys. Rev. D39 (1989) 187
11. T.K. Gaisser, F. Halzen, A.D. Martin: Phys. Lett. B166 (1986) 219
12. X.N. Wang: Phys. Rev. D43 (1991) 104
13. P. Danielewicz, G. Odyniec: Phys. Lett. B157 (1985) 146
14. H. Białkowska et al.: Phys. Lett. B173 (1986) 349
15. N. Agababyan et al., NA22 Coll.: Phys. Lett. B320 (1994) 411
16. M. Adamus et al., NA22 Coll.: Z. Phys. C32 (1986) 475
17. M. Adamus et al., NA22 Coll.: Z. Phys. C39 (1988) 311
18. M. Adamus et al., NA22 Coll.: Z. Phys. C37 (1988) 215
19. B. Andersson et al.: Nucl. Phys. B281 (1987) 289
20. B. Andersson et al.: Z. Phys. C57 (1993) 485
21. N.S. Amelin and L.V. Bravina: Sov. J. Nucl. Phys. 51 (1990) 133;
    N.S. Amelin, L.V. Bravina, L.N. Smirnova: Sov. J. Nucl. Phys. 52 (1990) 362
22. M.C. Foster et al.: Phys. Rev. D6 (1972) 3135
23. V.V. Aivazyan et al., NA22 Coll.: Z. Phys. C42 (1989) 533
24. C. De Marzo et al., NA5 Coll.: Nucl. Phys. B211 (1983) 375
25. T. Åkesson and H.-U. Bengtsson, Phys. Lett. 120B (1983) 233

Table 1. Average values of transverse momenta in the forward and backward hemispheres and in the central region

	total hemispheres		$\|x_F\| < 0.2$	
	$\langle Q_f \rangle$ GeV/c	$\langle Q_b \rangle$ GeV/c	$\langle Q_f \rangle$ GeV/c	$\langle Q_b \rangle$ GeV/c
experiment	1.028±0.004	0.974±0.003	0.936±0.004	0.885±0.004
QGSM	0.684±0.002	0.676±0.002	0.628±0.002	0.628±0.002
FRITIOF6.0	0.619±0.002	0.595±0.002	0.551±0.002	0.517±0.002
FRITIOF7.0	0.649±0.002	0.633±0.002	0.648±0.003	0.631±0.003

Table 2. Slopes of the $\langle Q_f(Q_b) \rangle$ and $\langle Q_b(Q_f) \rangle$-dependence (fit range 0.1 to 1.2 GeV/c)

	total hemispheres		$\|x_F\| < 0.2$	
	b_f	b_b	b_f	b_b
experiment	0.34 ± 0.03	0.37 ± 0.03	0.32 ± 0.03	0.32 ± 0.03
QGSM	0.31 ± 0.01	0.30 ± 0.01	0.17 ± 0.01	0.19 ± 0.01
FRITIOF6.0	0.18 ± 0.02	0.19 ± 0.02	0.09 ± 0.02	0.10 ± 0.02
FRITIOF7.0	0.32 ± 0.01	0.33 ± 0.01	0.17 ± 0.01	0.18 ± 0.01

Table 3. Slopes of the $\langle Q_f^2(Q_b^2)\rangle$ and $\langle Q_b^2(Q_f^2)\rangle$-dependence

	total hemispheres		$\lvert x_F\rvert < 0.2$	
	b_f	b_b	b_f	b_b
experiment	0.60 ± 0.06	0.74 ± 0.08	0.67 ± 0.08	0.63 ± 0.09
$\langle n_i(n_j)\rangle$	0.15 ± 0.02	0.15 ± 0.02		0.30 ± 0.01
QGSM	0.39 ± 0.002	0.38 ± 0.02	0.24 ± 0.02	0.26 ± 0.02
FRITIOF6.0	0.25 ± 0.02	0.27 ± 0.02	0.14 ± 0.01	0.14 ± 0.02
FRITIOF7.0	0.38 ± 0.01	0.39 ± 0.01	0.21 ± 0.01	0.21 ± 0.01

Table 4. Global characteristics of events with trigger ($p_T > 1.5$ GeV/c)

	σ (mb)	$\langle n\rangle$	$\langle p_{T,tr}\rangle$ GeV/c
experiment	0.0286 ± 0.0007	11.36 ± 0.09	1.75 ± 0.005
QGSM	0.0265 ± 0.0006	12.30 ± 0.06	1.75 ± 0.005
FRITIOF6.0	0.0021 ± 0.0002	10.50 ± 0.40	1.66 ± 0.01
FRITIOF7.0	0.0268 ± 0.0008	9.29 ± 0.12	1.78 ± 0.001

Figure Captions

Fig. 1 Distribution in the azimuthal angle $\Delta\varphi$ between the forward and backward transverse momentum vectors $\vec{Q}_f$ and $\vec{Q}_b$, in comparison to a statistical model described in the text (dotted), to FRITIOF6.0 (dot-dashed), FRITIOF7.0 (full) and QGSM (dashed).

Fig. 2 $\langle Q_f \rangle$ as a function of Q_b and $\langle Q_b \rangle$ as a function of Q_f, for all charged particles (upper diagrams) and those from the central region (lower), in comparison to FRITIOF6.0 (dot-dashed), FRITIOF7.0 (full) and QGSM (dashed).

Fig. 3 The average components $\langle p_{1,i} \rangle$ and $\langle p_{2,i} \rangle$ of the transverse momentum $\vec{p}_{T,i}$ in the direction of $\vec{Q}_{f,i}$ and $\vec{Q}_{b,i}$, respectively, as a function of rapidity y, compared to predictions from FRITIOF6.0 (dot-dashed), FRITIOF7.0 (full) and QGSM (dashed).

Fig. 4 The average component $\langle p_{x,i} \rangle$ of the transverse momentum $\vec{p}_{T,i}$ in the direction of $\vec{Q}_i$, as a function of rapidity y, compared to predictions from FRTIOF6.0 (dot-dashed), FRITIOF7.0 (full) and QGSM (dashed).

Fig. 5 Same as Fig. 3, but evaluated in the sphericity frame.

Fig. 6 Same as Fig. 4, but evaluated in the sphericity frame.

Fig. 7 Same as Fig.5, but for high-p_T trigger particles.

Fig. 8 Same as Fig. 6, but for high-p_T trigger particles.

Fig. 9 Transverse momentum flow per event as a function of Δy, separately for positive and negative particles, in trigger direction ($\Delta\varphi < \pi/2$) and opposite to the trigger direction ($\Delta\varphi > \pi/2$), in comparison to FRITIOF6.0 (dot-dashed), FRITIOF7.0 (full) and QGSM (dashed).

Fig. 10 $\langle p_T \cos\Delta\varphi \rangle$ per particle as a function of Δy, separately for positive and negative particles, in trigger direction ($\Delta\varphi < \pi/2$) and opposite to the trigger direction ($\Delta\varphi > \pi/2$), in comparison to FRITIOF6.0 (dot-dashed), FRITIOF7.0 (full) and QGSM (dashed).

Fig. 11 Average number of particles $\langle n \rangle$ as a function of Δy, separately for positive and negative particles, in trigger direction ($\Delta\varphi < \pi/2$) and opposite to the trigger direction ($\Delta\varphi > \pi/2$), in comparison to FRITIOF6.0 (dot-dashed), FRITIOF7.0 (full) and QGSM (dashed).

Fig. 12 Charge flow as a function of Δy, in trigger direction ($\Delta\varphi < \pi/2$) and opposite to the trigger direction ($\delta\varphi > \pi/2$), in comparison to FRITIOF6.0 (dot-dashed), FRITIOF7.0 (full line) and QGSM (dashed).

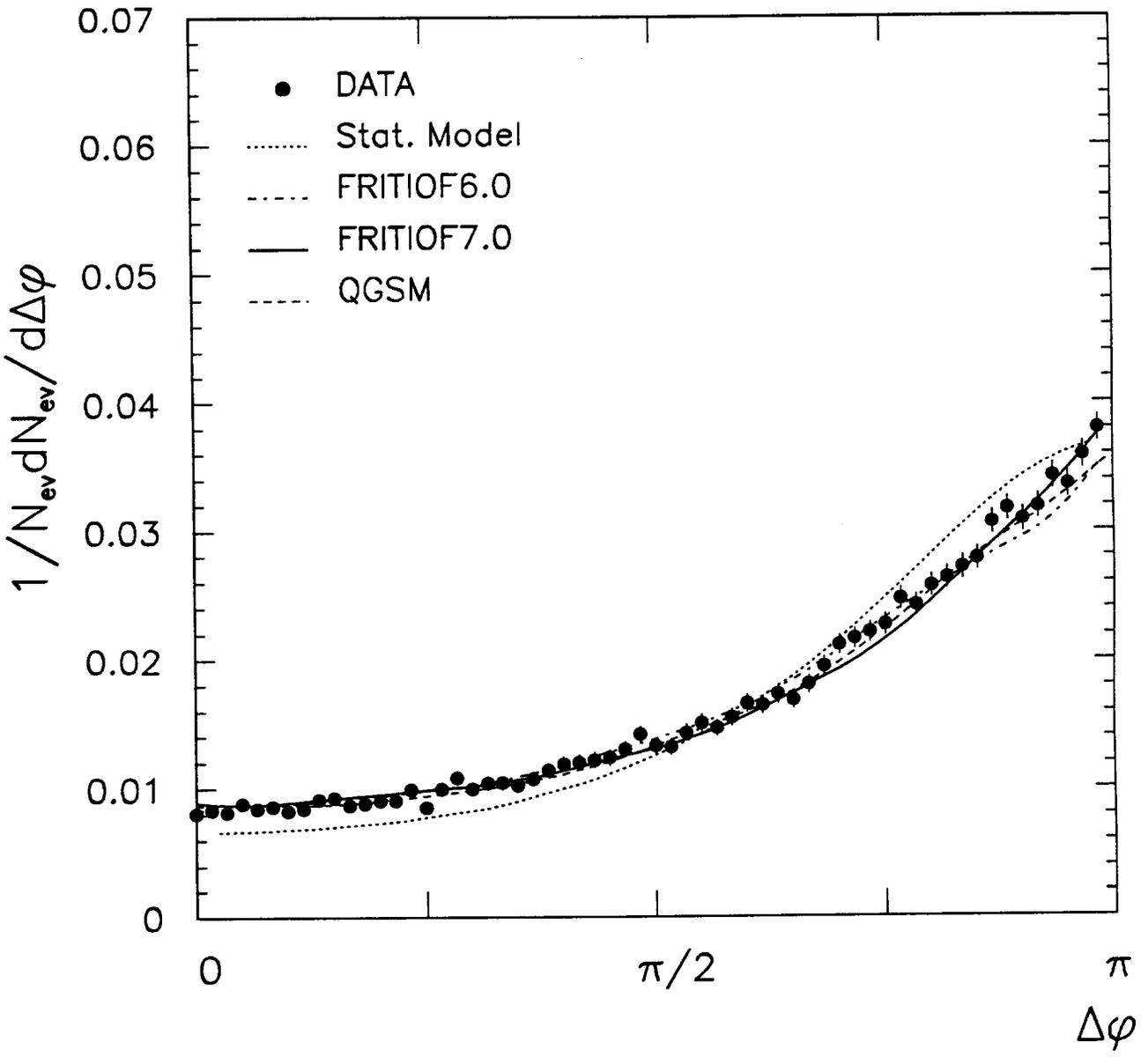
0.07
0.06
0.05
0.04
0.03
0.02
0.01
0
DATA
Stat. Model
FRITIOF6.0
FRITIOF7.0
QGSM
$1/N_{ev}dN_{ev}/d\Delta\varphi$
0
$\pi/2$
π
$\Delta\varphi$

Fig. 1

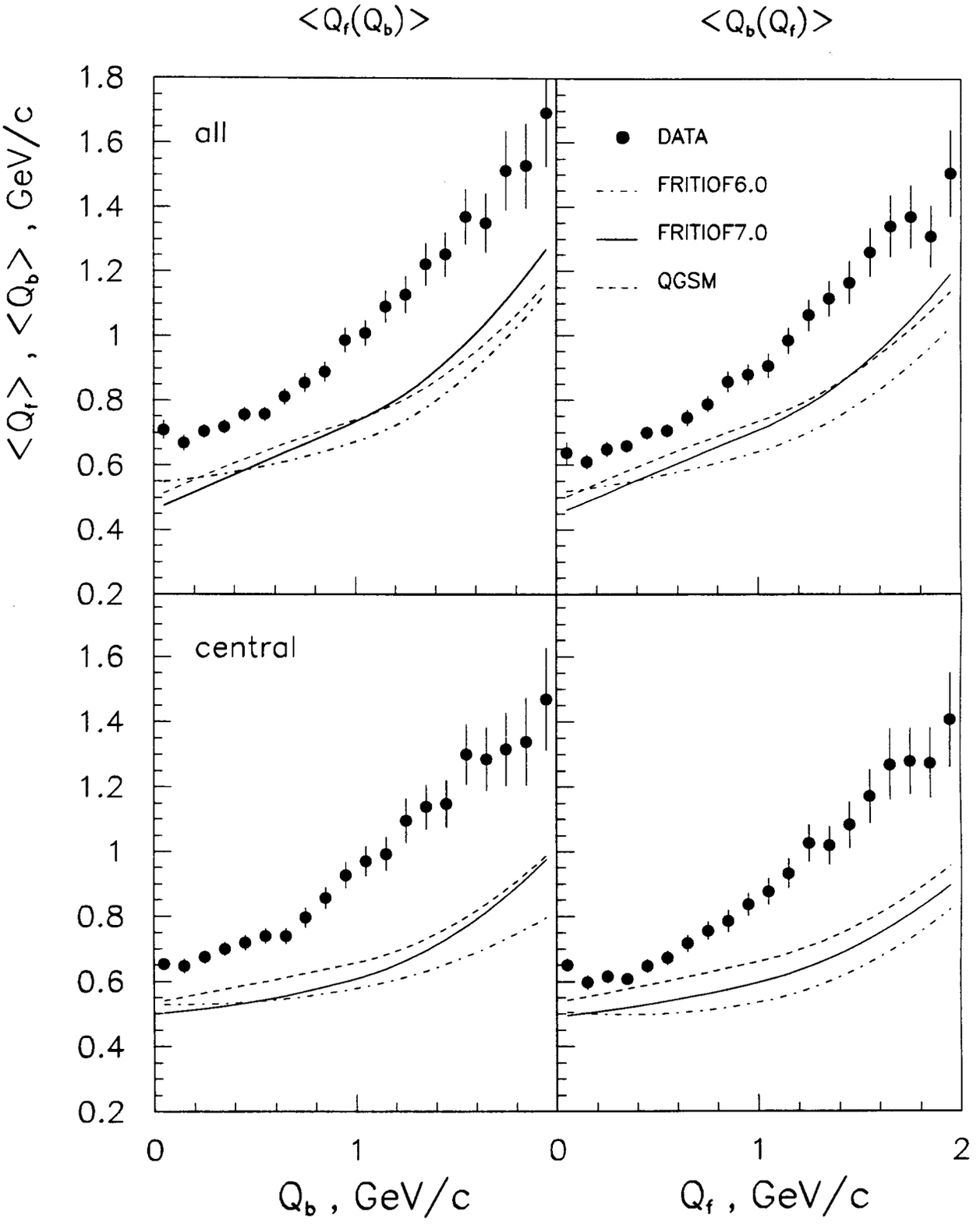
<Q_f(Q_b)>
<Q_b(Q_f)>
all
central
DATA
FRITIOF6.0
FRITIOF7.0
QGSM
<Q_f> , <Q_b> , GeV/c
Q_b , GeV/c
Q_f , GeV/c
0.2
0.4
0.6
0.8
1
1.2
1.4
1.6
1.8
0
1
2

Fig.2

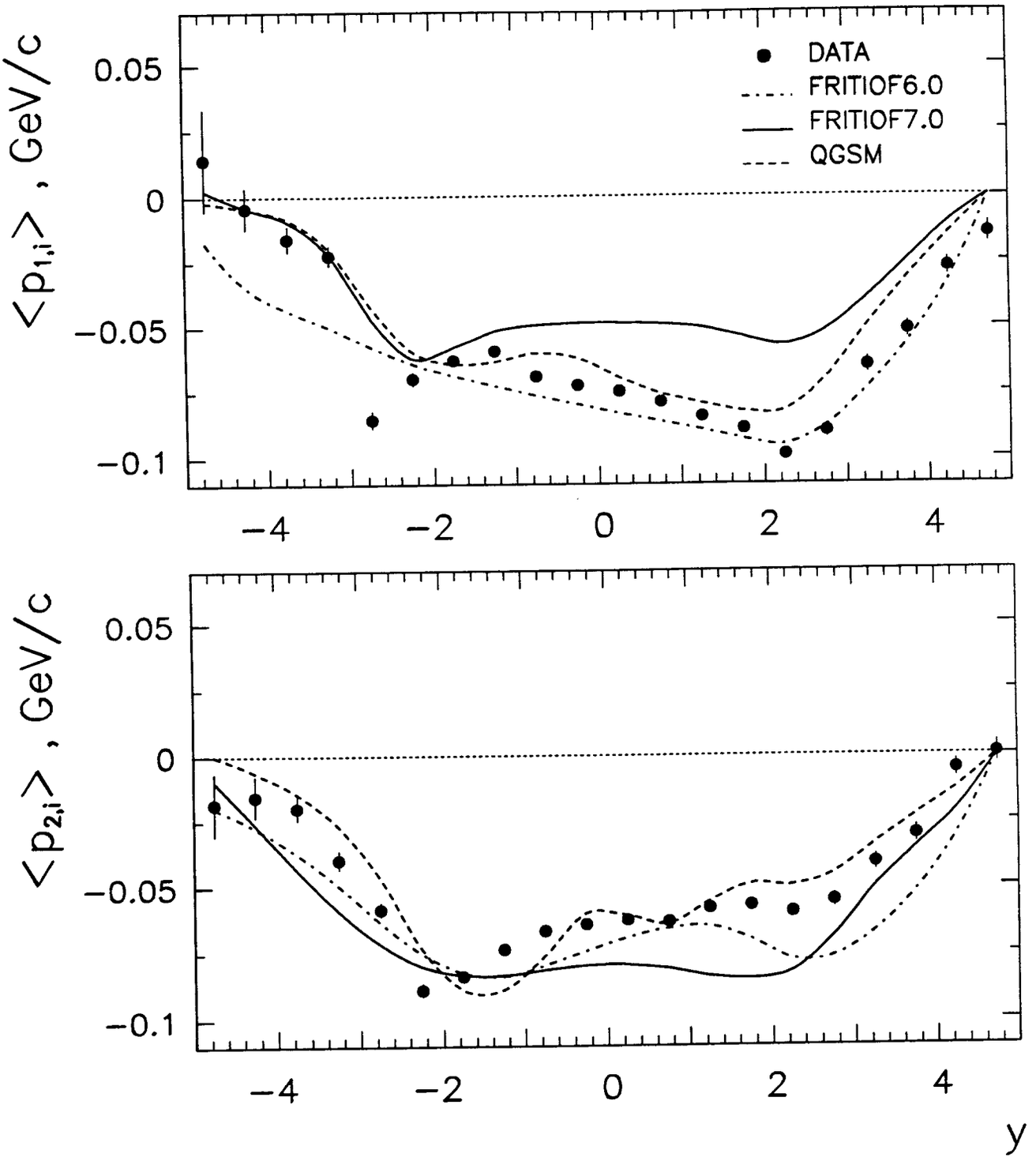
DATA
FRITIOF6.0
FRITIOF7.0
QGSM
<p1,i> , GeV/c
<p2,i> , GeV/c
0.05
0
−0.05
−0.1
−4
−2
0
2
4
y

Fig.3

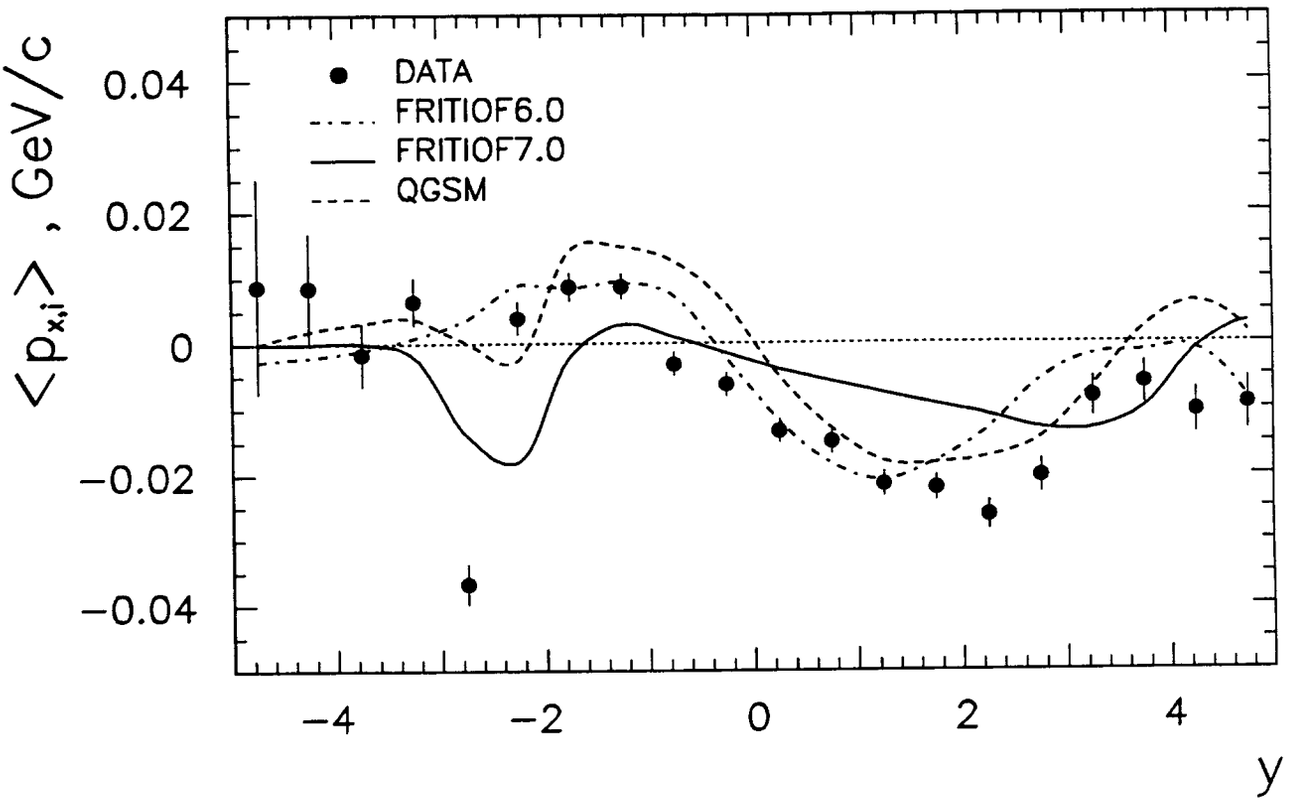
DATA
FRITIOF6.0
FRITIOF7.0
QGSM
0.04
0.02
0
−0.02
−0.04
−4
−2
0
2
4
y
<p_{x,i}> , GeV/c

Fig.4

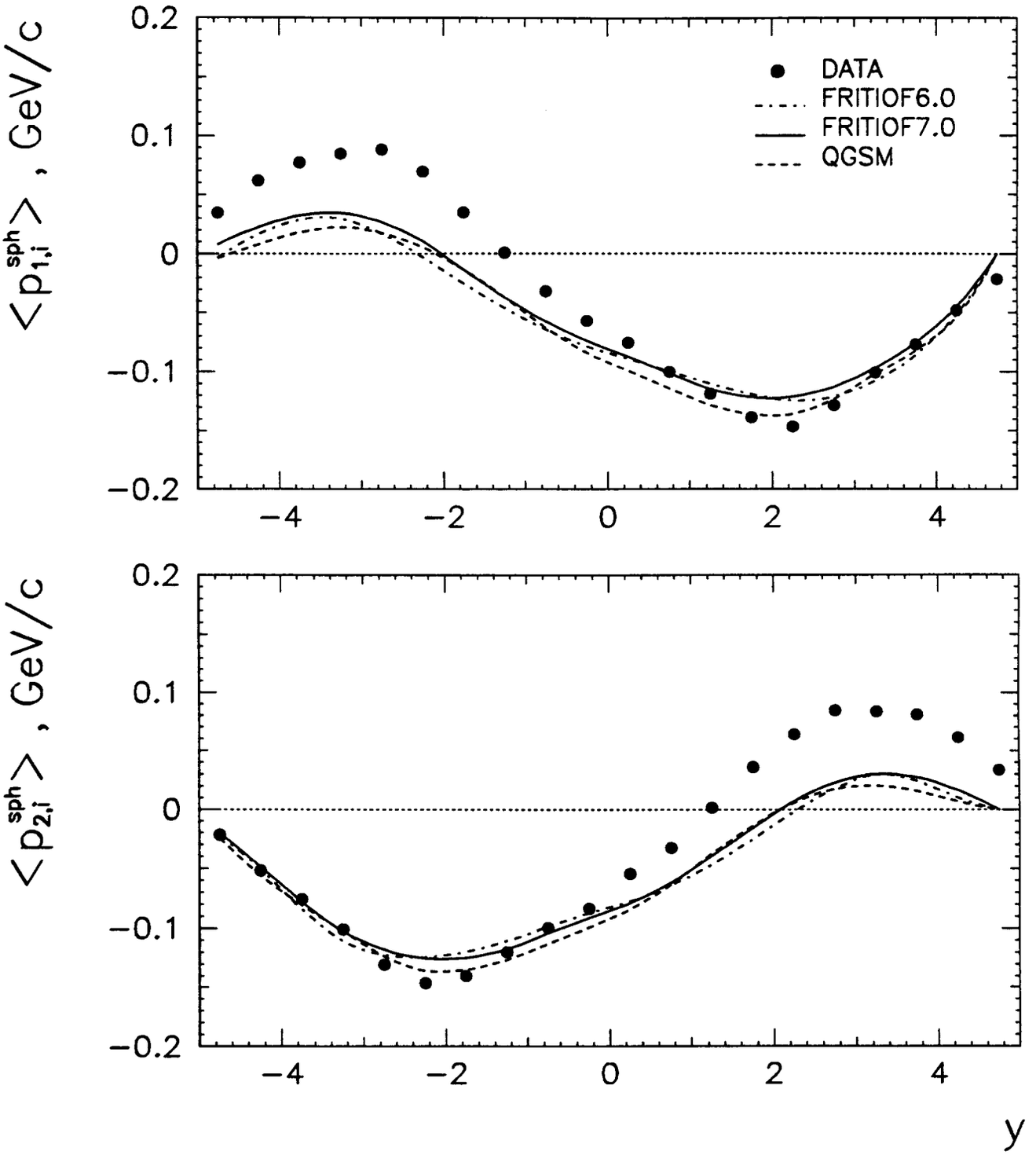
DATA
FRITIOF6.0
FRITIOF7.0
QGSM
$\langle p_{1,i}^{sph} \rangle$, GeV/c
$\langle p_{2,i}^{sph} \rangle$, GeV/c
0.2
0.1
0
−0.1
−0.2
−4
−2
0
2
4
y

Fig.5

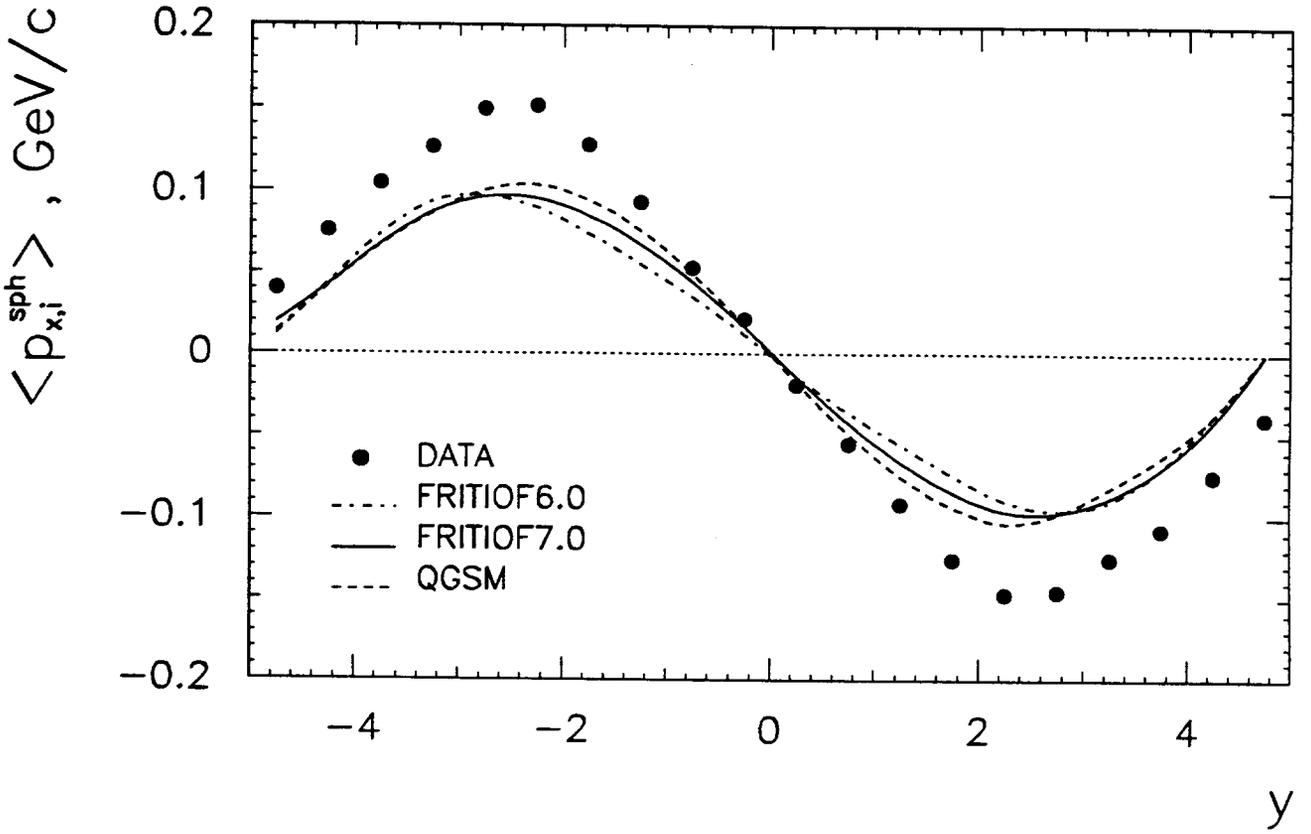
0.2
0.1
0
−0.1
−0.2
−4
−2
0
2
4
y
$\langle p_{x,i}^{sph} \rangle$, GeV/c
DATA
FRITIOF6.0
FRITIOF7.0
QGSM

Fig.6

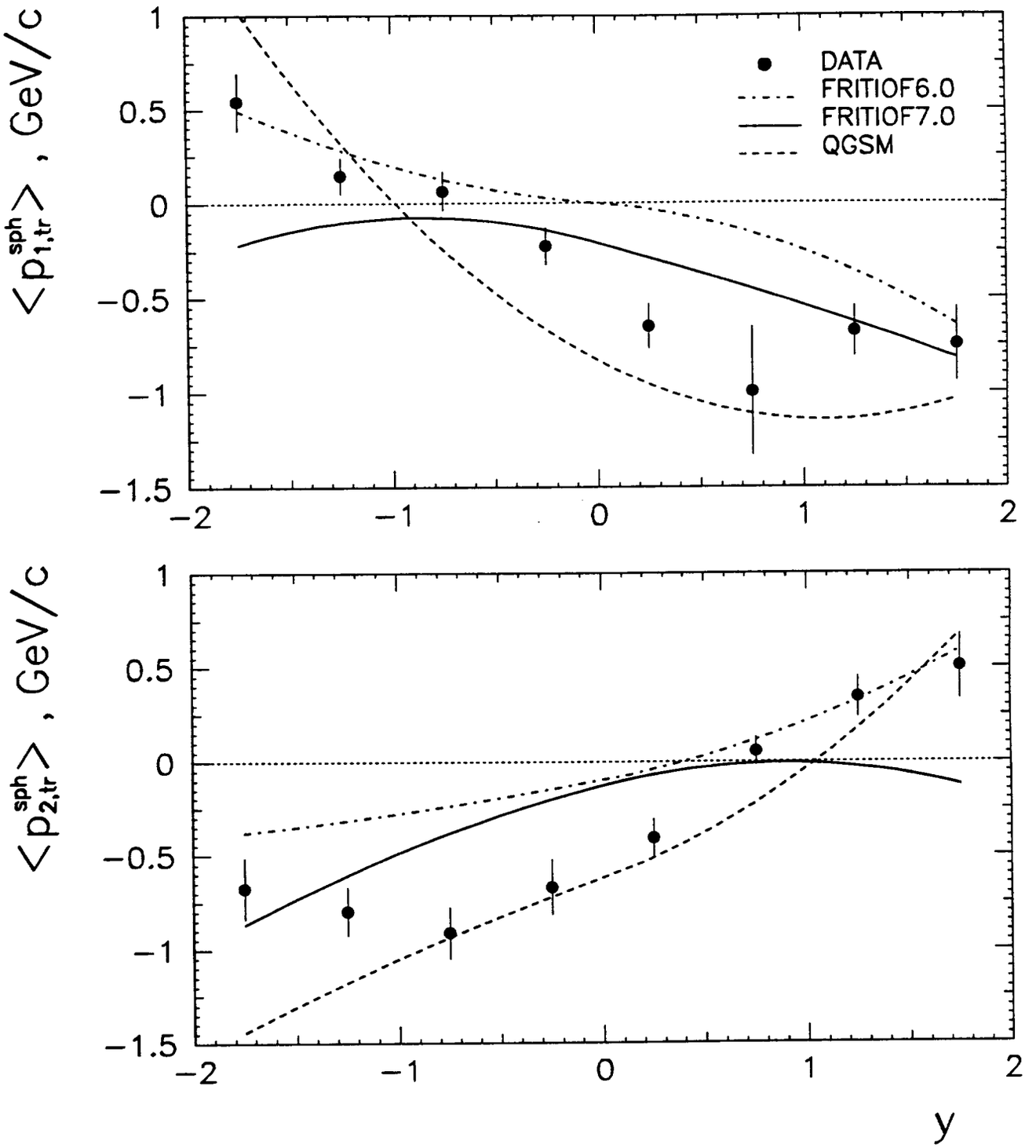
DATA
FRITIOF6.0
FRITIOF7.0
QGSM
$\langle p_{1,tr}^{sph} \rangle$, GeV/c
$\langle p_{2,tr}^{sph} \rangle$, GeV/c
y

Fig.7

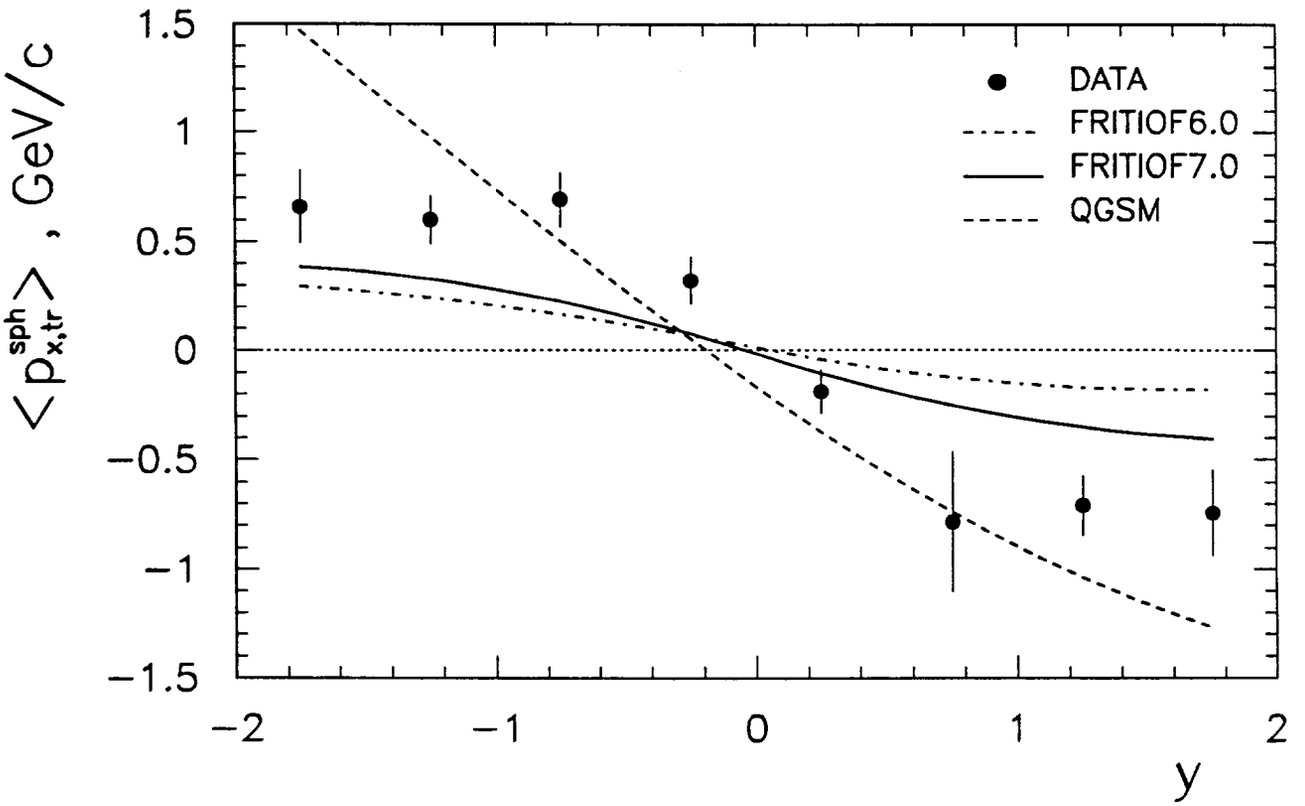
1.5
1
0.5
0
−0.5
−1
−1.5
−2
−1
0
1
2
y
$\langle p_{x,tr}^{sph} \rangle$, GeV/c
DATA
FRITIOF6.0
FRITIOF7.0
QGSM

Fig.8

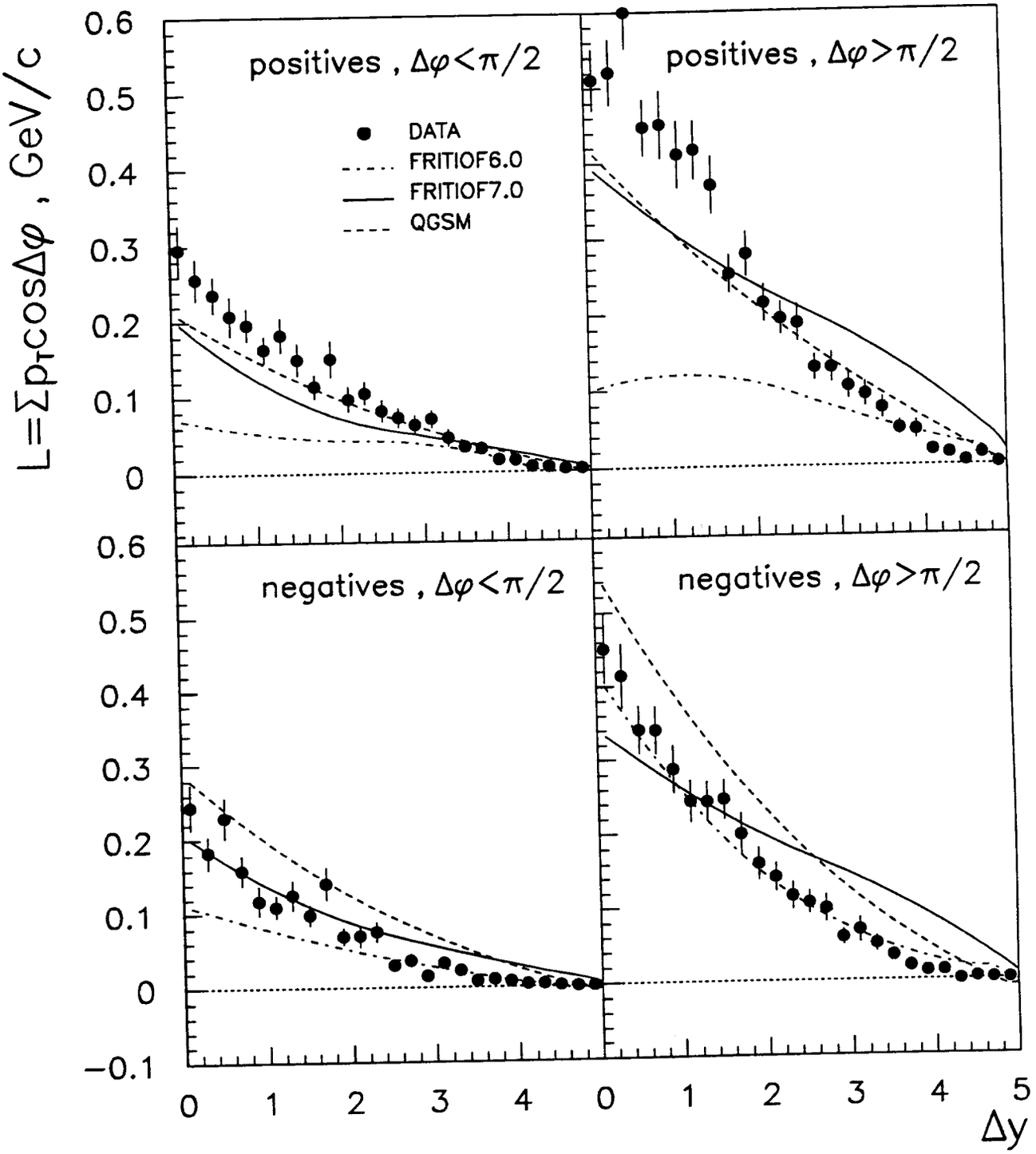
positives , Δφ<π/2
positives , Δφ>π/2
negatives , Δφ<π/2
negatives , Δφ>π/2
DATA
FRITIOF6.0
FRITIOF7.0
QGSM
L=Σp_T cosΔφ , GeV/c
Δy
0.6
0.5
0.4
0.3
0.2
0.1
0
−0.1
0
1
2
3
4
5

Fig.9

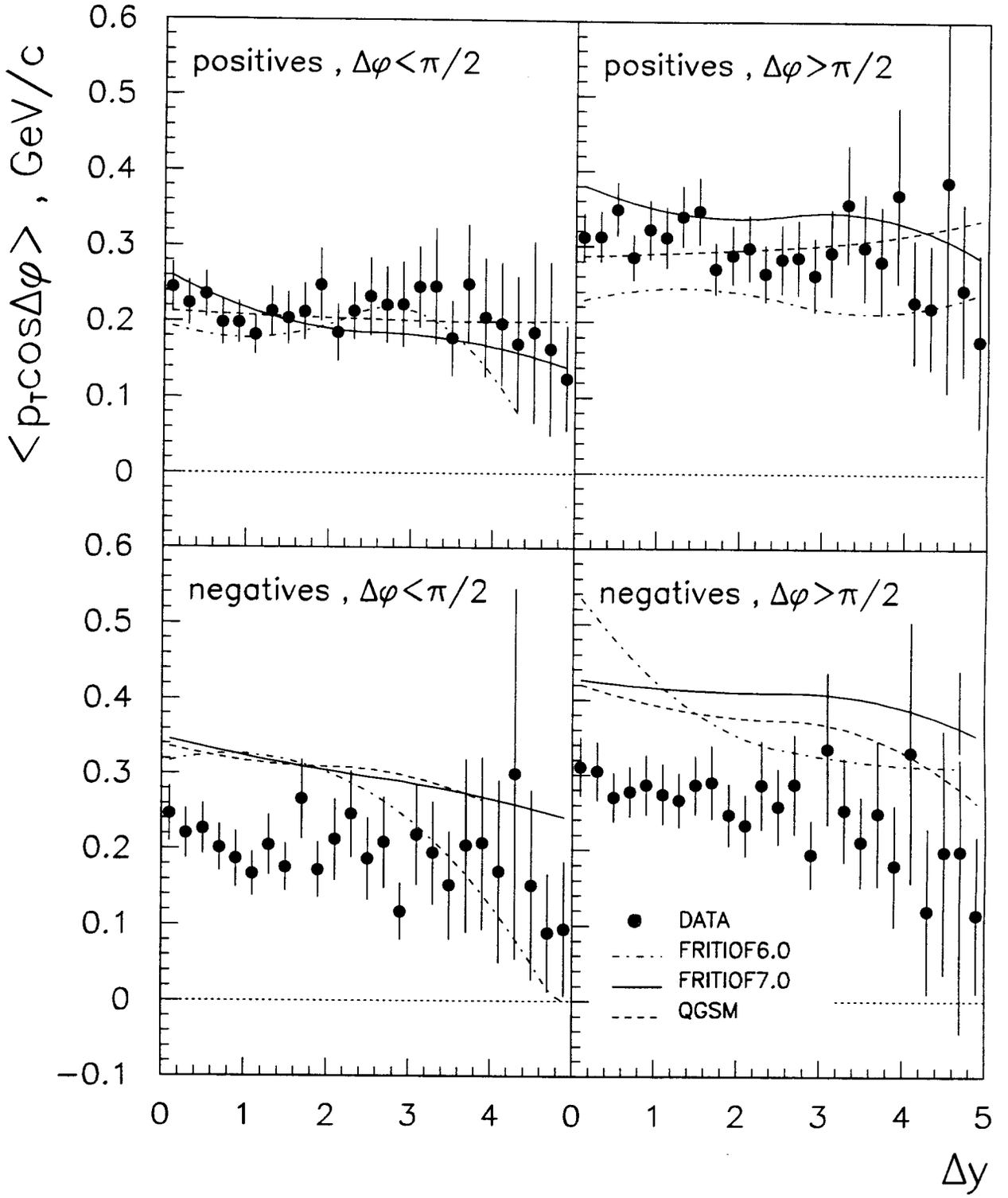
positives , Δφ<π/2
positives , Δφ>π/2
negatives , Δφ<π/2
negatives , Δφ>π/2
DATA
FRITIOF6.0
FRITIOF7.0
QGSM
<p_T cosΔφ> , GeV/c
Δy
0.6
0.5
0.4
0.3
0.2
0.1
0
−0.1
0
1
2
3
4
5

Fig.10

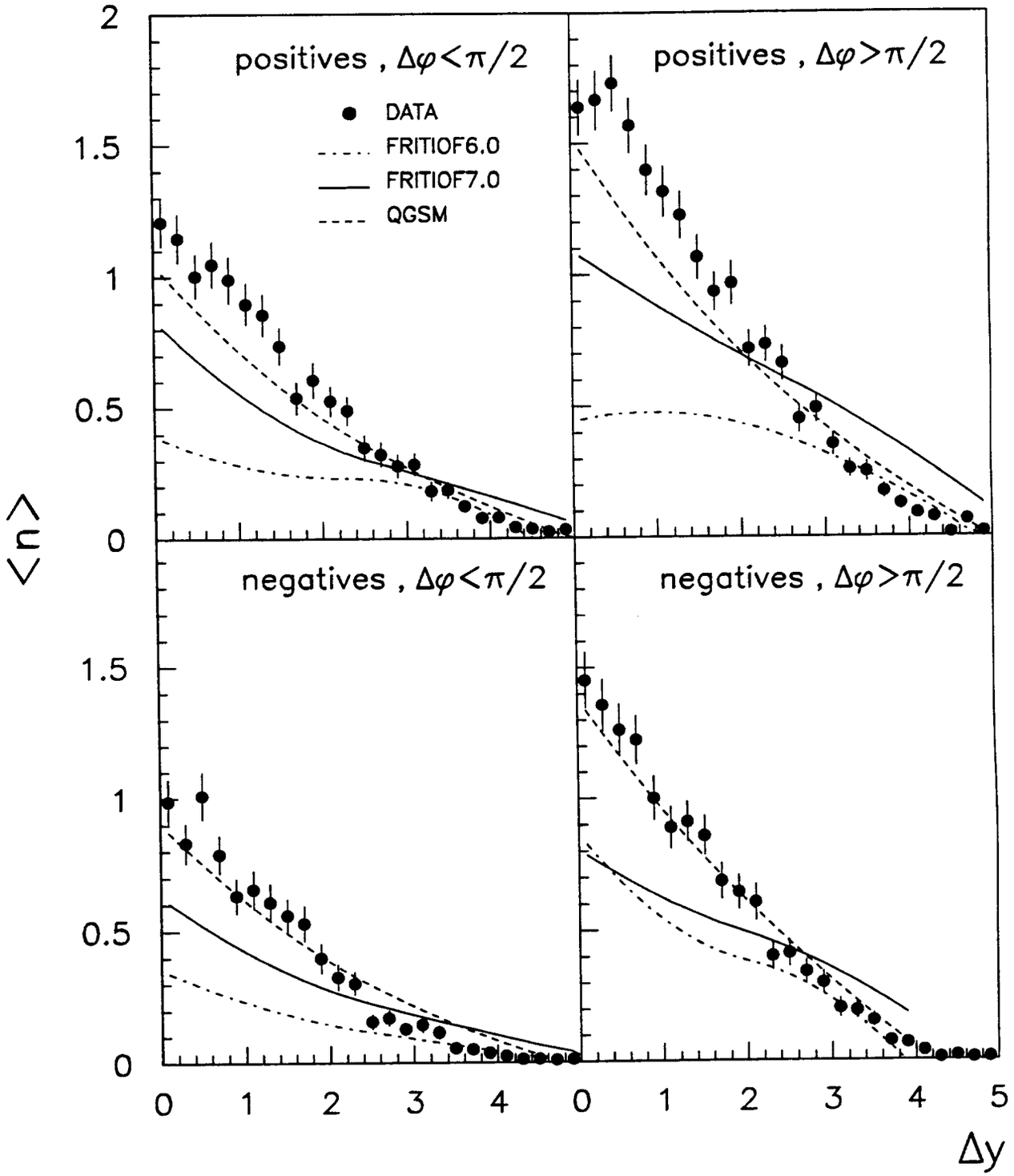
positives , Δφ<π/2
positives , Δφ>π/2
negatives , Δφ<π/2
negatives , Δφ>π/2
DATA
FRITIOF6.0
FRITIOF7.0
QGSM
<n>
Δy
0
0.5
1
1.5
2
0
1
2
3
4
5

Fig.11

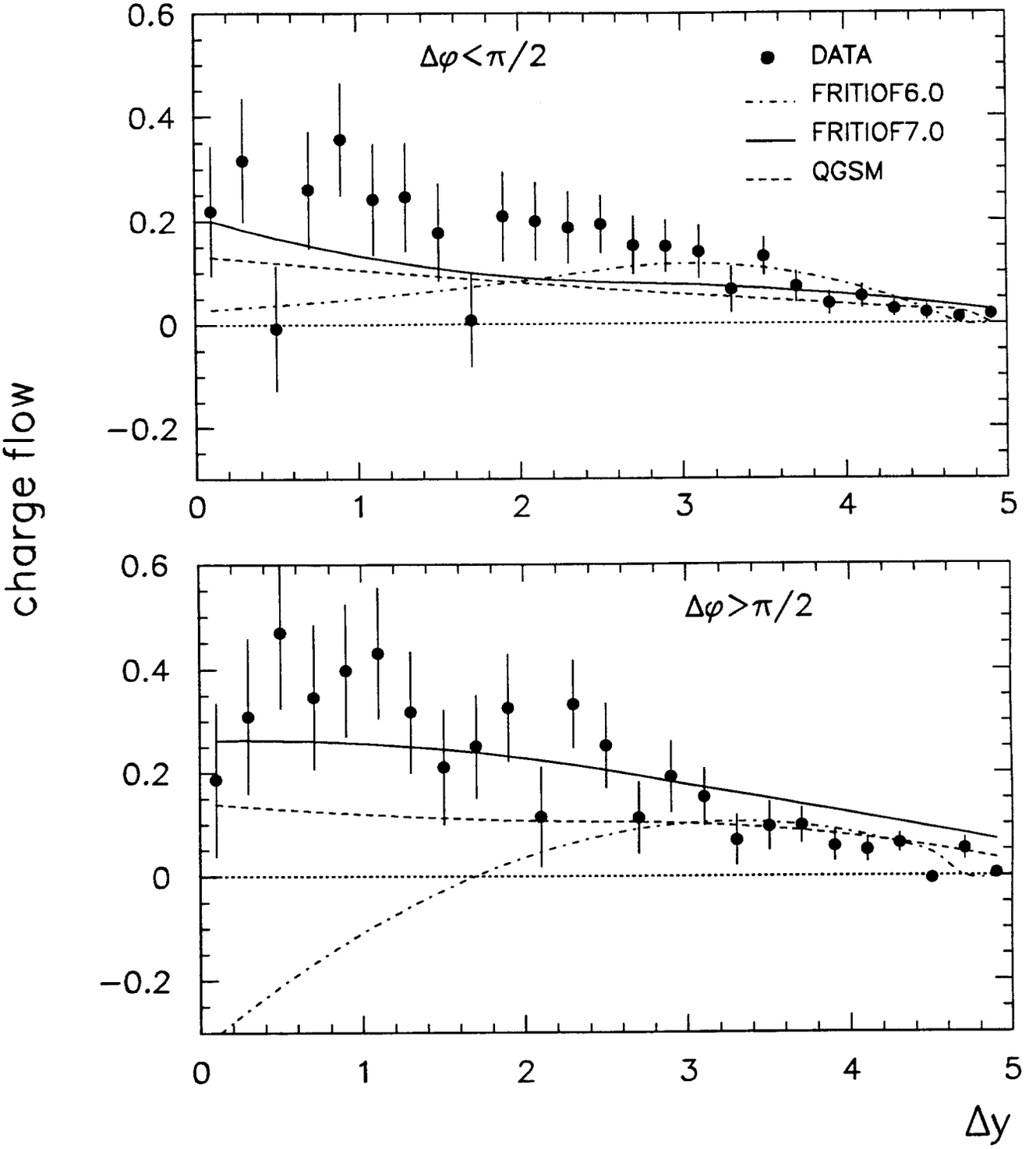
charge flow
Δφ<π/2
DATA
FRITIOF6.0
FRITIOF7.0
QGSM
Δφ>π/2
0.6
0.4
0.2
0
−0.2
0
1
2
3
4
5
Δy

Fig.12